IL NUOVO CIMENTO **41 C** (2018) 216
DOI 10.1393/ncc/i2018-18216-3

COLLOQUIA: SIRR 2018

On the use of highly pixellated CMOS imagers to measure therapeutic beam profile

L. SERVOLI(1)(*), L. ALUNNI SOLESTIZI(1), M. BIASINI(1)(2), S. FABIANI(3), M. ITALIANI(3), K. KANXHERI(1) and P. TUCCERI(1)

(1) *INFN, Sezione di Perugia - Perugia, Italy*
(2) *Dipartimento di Fisica e Geoologia, Università di Perugia - Perugia, Italy*
(3) *Azienda Ospedaliera S. Maria - Terni, Italy*

received 4 December 2018

Summary. — The characterization of high-intensity charged-particle and photon beams at medical accelerators is often a time-consuming task. In this work, we discuss the possibility to use highly segmented CMOS imagers as a way to measure the fluxes with high spatial precision and in a short time. Quite recently CMOS imagers, designed to collect visible light, have been used to detect ionizing radiation, either charged particles (electron, proton) or photons. These devices, due to the very low single pixel noise, have a very high detection efficiency, once the interaction between radiation and silicon has taken place, and act primarily as counting detectors. We will show how it is possible to extract a precise beam shape using as a test case a therapeutic electron beam delivered by an Elekta e-LINAC at the S. Maria Hospital in Terni (Italy), and as sensors commercial off-the-shelf (COTS) CMOS imagers.

1. – CMOS imagers as ionizing radiation detectors

The characterization of charged particle beams, either for medical purposes or industrial ones, is an important subject, and the availability of new sensors is always sought to increase the precision of the measurements and reduce the time and the effort needed. In particular flux measurement is essential to define the beam shape, including penumbra regions that are often difficult to define precisely due to the rapidly varying radiation field and the dimension of the sensor. In this work the capability of commercial off-the-shelf (COTS) CMOS imagers as detectors for measuring the flux of charged particles will be explored.

CMOS imagers, optimized for visible light collection, mainly produced by Aptina, have been used in the past years as ionizing radiation detectors either for photons or

(*) Corresponding author. E-mail: leonello.servoli@pg.infn.it

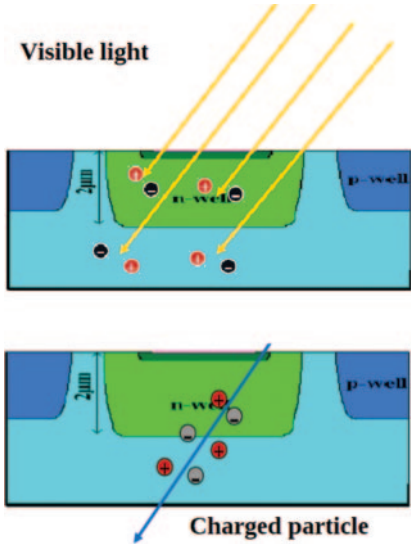

Fig. 1. – CMOS imager signal formation: (top) visible light: each photon creates an electron-hole pair; (bottom) a single charged particle creates many electron-hole pairs.

for charged particles [1-6]. The reason for this growing interest lies in the very high S/N that a charged particle produces in the sensitive layer of the devices. Due to the request of being capable of making pictures even in very poor light condition, (low signal level), these types of sensors are forced to have a very low pixel noise, of the order of few electrons, to enhance the S/N ratio even in all cases.

In fig. 1 the two different energy deposition mechanisms for the case of visible light and single charged particle crossing the sensitive layer are shown. In the first case, the number of electron-hole pairs produced is proportional to the number of incoming photons, focused by the microlens over the pixel, arriving within the exposure time (integration time from now on), while in the latter case the number of created electron-hole pairs depends on the thickness of the sensitive layer, on the momentum of the incoming particle and on the portion of the track that lies below the single pixel. Given the typical thickness of few μm of the sensitive layer and the worst signal formation case, the minimum ionizing particle (MIP), the number of pairs created is of the order of 50–200. Coupled with the very low noise (∼2–3 electrons for standard 33 ms integration time), this produces a S/N $>$ 20 when the pixel photodiode collects all electrons. Another difference is that, due to the production process, the layer containing the CMOS electronics (1 μm thickness) has dead regions, while the epitaxial layer below (sensitive layer with few μm thickness) is homogeneous across all matrix area. Hence, given the thickness of the two layers, this class of sensors has no dead space and a slightly variable sensitive volume. It has been demonstrated that the reduction in charge collection efficiency in the first layer is of the order of 25% [7, 8], thus keeping a very high S/N in all cases.

If the path of the incoming charged particle is close to the border of the pixel or if the amount of created electron-hole pairs is very high (low-energy electrons, protons, α), the electrons could be collected by more than one pixel at a level that is greater than the noise level for each pixel. See, for example, fig. 2, where a 450 MeV electron creates a cluster with few pixels having signal above the noise level (left) while a 3 MeV proton

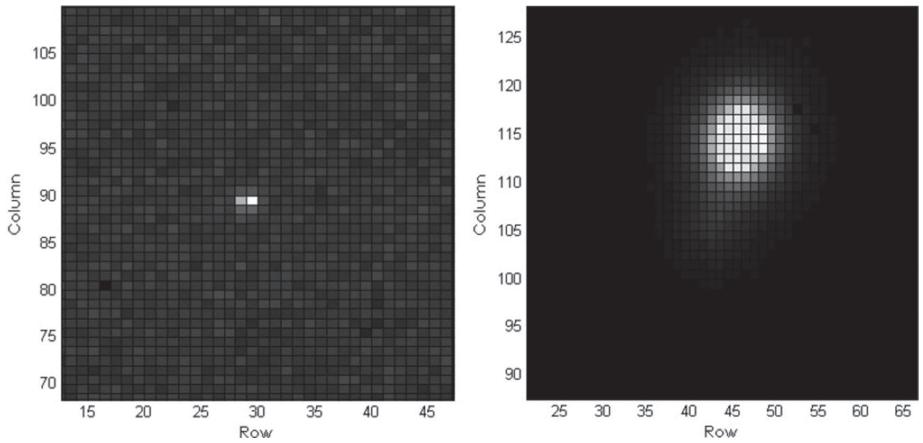

Fig. 2. – Image of isolated clusters. Left: minimum ionizing particle (450 MeV electron). Right: highly ionizing particle (3 MeV proton).

(right) creates a cluster of ∼100 pixels over the noise. Because each pixel produces an analog signal, with ADC conversion done directly on the sensor at the periphery of the pixel matrix, the signal division among adjacent pixels could be used to better identify the incoming particle through several types of clustering algorithms that reconstruct both energy deposition and impact position of the charged particle [2].

The very high pixel density (∼0.25 Mpixel/mm^2) makes this class of detectors ideal for single-cluster counting for MIPs up to quite high fluxes. A single cluster has almost always a pixel with more signal than the others, thus a topology of a local maximum, hence to count the number of such maxima in a frame, is a direct measurement of the flux of incoming charged particles if a detection efficiency close to 100% can be assumed, as is when a S/N $>$ 20 is reached. The only problem lies in the superposition among two or more different clusters that results in cluster merging (decrease of cluster number) or creation of fake maxima when two or more contributions sum up on a pixel belonging to the periphery of the clusters, causing a cumulative signal greater than the neighboring ones (increase of the cluster number). These problems could cause a deviation from linearity of the relation between incoming particles and detected clusters.

Taking advantage of the high pixel density and also of the high multiplicity of incoming beams, a non-linear calibration procedure has been developed [9] allowing to reach a precision better than 1% in flux measurement in a range of ∼10 MHz/cm^2, depending on the pixel size of the CMOS imager and on the thickness of the epitaxial layer.

2. – Electron flux measurement

A measurement campaign on a clinic accelerator (Electa e-LINAC) located at S. Maria Hospital in Terni (Italy) has been carried out to study the CMOS imager capability to measure the electron flux. The horizontal position of the accelerator allowed an easier positioning of the mechanical setup (fig. 3). The electron beam parameters were set at 10 MeV, 50 MU, 160 s irradiation time, while the sensor was placed at the beam center at a distance of 140 cm from the beam exit window. Two precision linear stages (each step is 210 nm) were connected to obtain x-y movements in the plane orthogonal to the beam direction and a plastic holder was used to support the CMOS imager under test.

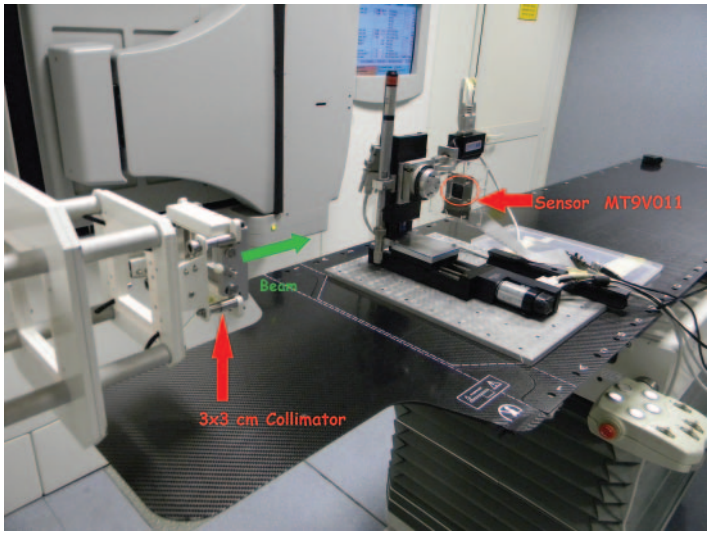

Fig. 3. – experimental setup on the Elekta e-LINAC in S. Maria Hospital (Terni): beam coming from left (greeen arrow), precision x-y movements and CMOS imager on its holder.

Several sensors from Aptina were used, as detailed in table I, to perform different tests. Each sensor was located in its evaluation board and readout using a DAQ board (Aptina Demo2 or Demo2X) with an FPGA to control the sensor and to receive and process the data, to be sent via a USB 2.0 connection to a PC for frame storing ([10]). The measurement sequence for each experimental point is the following:

- the DAQ is started before switching on the beam, to have some frames without beam;
- the beam is switched on and left running for 180 s;
- the beam is switched off;
- the DAQ is stopped.

Then, for each frame, the number of relative maxima is found and plotted as a function of the frame number (the time), then converted into flux measurement and used to build the distribution of the flux measurements for all frames (inset in fig. 4). This distribution is essentially Gaussian due to the randomness of the occupancy on the sensor surface

TABLE I. – *List of CMOS imagers under study and their main characteristics.*

Sensor	MT9V011	MT9T031	MT9J003
Number of pixels	307200	3145728	10068672
Pixel area (μm^2)	31.36	10.24	2.7889
Pixel size (μm)	5.6	3.2	1.67
Epi-region thickness (μm)	4.0	4.0	4.0

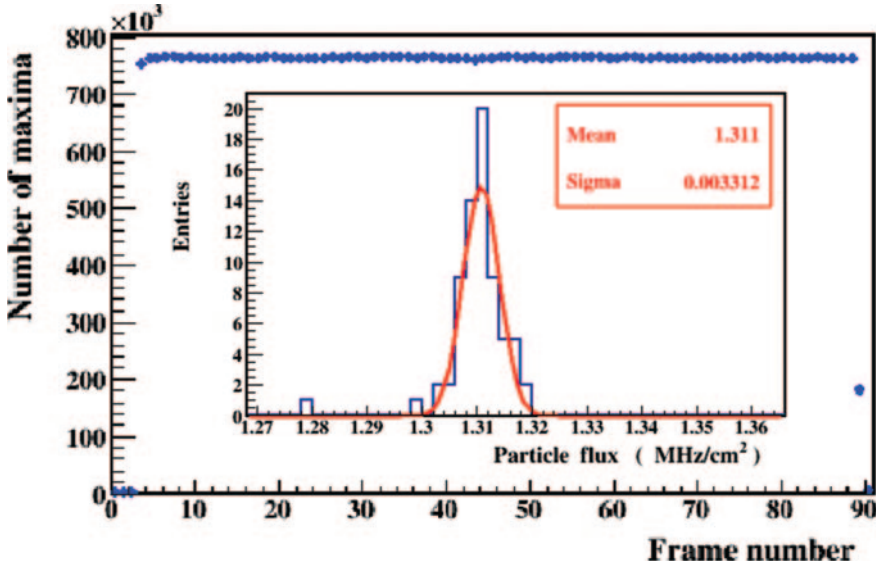

Fig. 4. – N_{maxima} *vs.* number of frame for the MT9J003 sensor on 10 MeV, 50 MU, $3 \times 3\,\mathrm{cm}^2$ collimator electron beam from Elekta e-LINAC. Inset: distribution of flux measurements after applying non-linear calibration.

and its variation is a measure of the precision of the flux measurements. In this case the relative uncertainty is 0.25%, while the accuracy is within the uncertainty of the signal measured by the control system, *i.e.*, the silicon microstrip system [11].

The first set of measurements, using MT9T031 and MT9J003 reported in [9], confirmed the validity of the non-linear calibration technique to measure the electron flux, giving results compatible within uncertainties and compatible also with the control measurement performed using silicon microstrips.

3. – Beam profile measurement

To measure the beam profile a position scan in both x-y coordinates (x has a 100 mm range, y a 50 mm range) has been performed using the sensor MT9V011. The row coordinate of the sensor is along the y-axis and the column coordinate is along the x-axis. The measurement procedure was organized as follows:

- for each point of the scan 15 frames were acquired (3 seconds);
- the distance from two consecutive points is 5 mm;
- beam and DAQ always on;
- x scan from $[-50, 0]$ position until $[+50, 0]$;
- y scan from $[-25, 0]$ position until $[+25, 0]$;

The beam profile scan was completed in less than 5 minutes, all considered. In fig. 5 the sequence of flux measurements is reported as a function of the frame number during

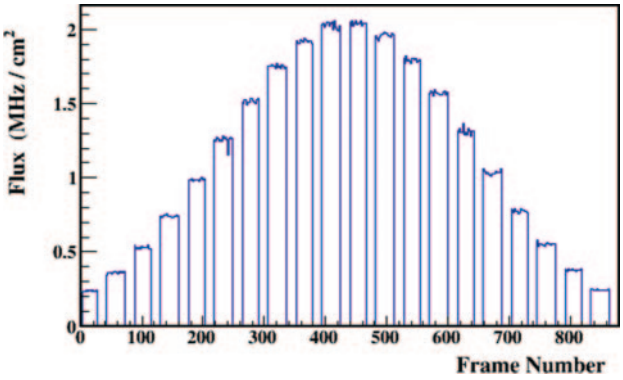

Fig. 5. – Electron flux *vs.* number of frame for MT9V011 during position scan.

the x-coordinate scan. Then, for each measurement point, the average of the measurement distribution and its relative RMS have been extracted (fig. 6).

The position of each point of the scan is fixed at the center of the sensor, hence each measurement point has a width along the x-coordinate of ± 1.79 mm, defining the granularity of the measurement and its precision in that coordinate. The shape of the beam is approximately Gaussian-like, as expected, and its width is $\sim$23 mm. Concerning the relative uncertainties, we have obtained approximately the same results reported in [9] where an uncertainty of 1% in flux measurement was predicted for the MT9V011 sensor at 2.14 MHz/cm^2 flux. The position scan in the y-coordinates, even if performed on a 50 mm range instead than 100 mm, gave similar results with a width of the distribution of 24.6 mm, confirming the symmetry of the beam around the beam axis.

4. – Sensor segmentation

A further possibility given by the very high segmentation is to subdivide the matrix in $N \times M$ submatrices and perform $N \times M$ flux measurements at the same time in an area of $\sim$10 mm^2. The area is wide enough to record flux variations in position between one submatrix and the others. That would allow a much finer shape measurement at a possible price of increasing the uncertainty for each flux measurement. In fact, the uncertainty will depend on the number of maxima present in the submatrix area, depending

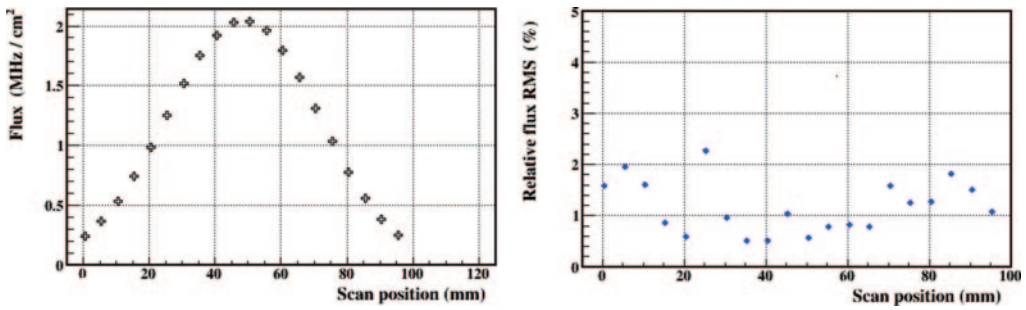

Fig. 6. – Left: electron flux *vs.* position for MT9V011 during position scan. Right: relative flux RMS for each measurement point.

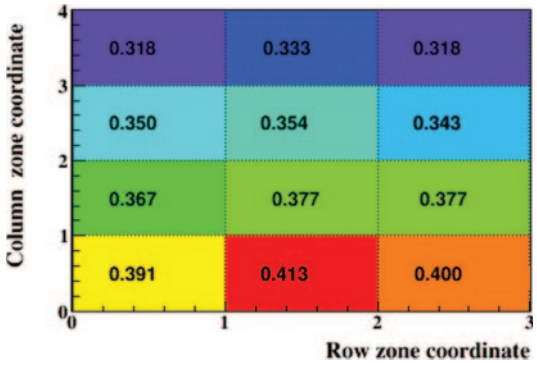

Fig. 7. – Map of the flux measurement for a subdivision into 3×4 submatrices, 150×150 pixel wide at point 10 mm of the position scan along the x-coordinate.

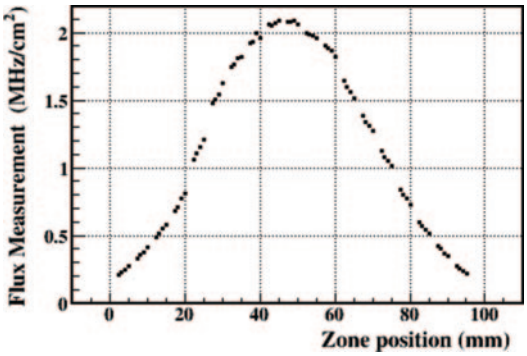

Fig. 8. – Beam shape along the x-coordinate for the MT9V011 sensor subdivided into 3×4 submatrices, 150×150 pixel wide, using the central submatrices of the y-coordinate (row coordinate) in fig. 7.

hence on the number of pixels that form the area. Choosing a square submatrix with a 150 pixels side, with 1% relative uncertainty, 12 submatrices are formed. Studying the flux measurements on them at a point in the scan where there is a rapid variation of the flux, for example the 5 mm point, the sensor capability to measure flux differences is confirmed as shown in fig. 7.

The variation in flux is present on the x-coordinate (column coordinate) (10% difference over 3.5 mm, with 1% uncertainty on each point) but not on the y-coordinate (row coordinate) with 2% over 1.3 mm. The slope of the flux variation is essentially the same on all the slices on the x-coordinate, thus confirming the capability to perform measurements over a limited sensor surface ($0.7\,\mathrm{mm}^2$) with an uncertainty of the order of 1% (fig. 8).

5. – Conclusions

Highly pixellated COTS CMOS imagers could be used to characterize therapeutic electron beams provided a proper non-linear calibration is performed. The shape of the beam could be precisely determined, with uncertainty in each measurement point of the order of 1% or less.

Moreover, a subdivision of the sensor surface in smaller submatrices with at least a 150 pixel side could provide multiple measurement points for a better shape mapping. In principle, the submatrix area could be reduced if we use sensors with smaller pixel size, like $2 \times 2\,\mu\text{m}^2$ to $0.4\,\text{mm}^2$ keeping the same 1% uncertainty on the measurement points. Further investigations are needed to understand if the beam shape determination could be done in just one DAQ session varying also the z position of the sensor and to assess the stability in time of the sensor response.

* * *

This work is partially supported by Fondazione Cassa di Risparmio di Perugia: Project RIPARI n. 2017.0104.021.

REFERENCES

[1] Servoli L., Biagetti D., Passeri D. and Spanti Gattuso E., *IEEE Nuclear Science Symposium Conference Record, NSS08* (IEEE) 2008, pp. 2484–2488.
[2] Servoli L., Biagetti D., Passeri D. and Spanti Gattuso E., *J. Instrum.*, **5** (2010) P07003.
[3] Servoli L., Biagetti D., Meroli S., Placidi P., Passeri D. and Tucceri P., *Nucl. Phys. B Proc. Suppl.*, **215** (2011) 228.
[4] Castoldi A., Guazzoni C., Maffessanti S., Montemurro G. V. and Carraresi L., *J. Instrum.*, **10** (2015) C01002.
[5] Perez M. *et al.*, *Nucl. Instrum. Methods A*, **827** (2016) 171.
[6] Holden W. M., Hoidn O. R., Seidler G. T. and DiChiara A. D., *Rev. Sci. Instrum.*, **89** (2018) 093111.
[7] Meroli S., Biagetti D., Passeri D., Placidi P., Servoli L. and Tucceri P., *Nucl. Instrum. Methods A*, **650** (2011) 230.
[8] Meroli S., Passeri D. and Servoli L., *J. Instrum.*, **6** (2011) P06013.
[9] Servoli L. and Tucceri P., *J. Instrum.*, **11** (2016) P03014.
[10] `http://www.aptina.com/`.
[11] Alpat B., Pilicer E., Servoli L., Menichelli M., Tucceri P., Italiani M., Buono E. and Di Capua F., *J. Instrum.*, **7** (2012) P03013.